PERGAMON

Engineering Failure Analysis 9 (2002) 63–76

ENGINEERING FAILURE ANALYSIS

www.elsevier.com/locate/engfailanal

Thermal cracking in disc brakes

Thomas J. Mackin *,[1], Steven C. Noe, K.J. Ball, B.C. Bedell, D.P. Bim-Merle, M.C. Bingaman, D.M. Bomleny, G.J. Chemlir, D.B. Clayton, H.A. Evans, R. Gau, J.L. Hart, J.S. Karney, B.P. Kiple, R.C. Kaluga, P. Kung, A.K. Law, D. Lim, R.C. Merema, B.M. Miller, T.R. Miller, T.J. Nielson, T.M. O'Shea, M.T. Olson, H.A. Padilla, B.W. Penner, C. Penny, R.P. Peterson, V.C. Polidoro, A. Raghu, B.R. Resor, B.J. Robinson, D. Schambach, B.D. Snyder, E. Tom, R.R. Tschantz, B.M. Walker, K.E. Wasielewski, T.R. Webb, S.A. Wise, R.S. Yang, R.S. Zimmerman

Department of Mechanical and Industrial Engineering, The University of Illinois at Urbana-Champaign, 1206 West Green Street, Urbana, IL 61802, USA

Received 29 August 2000; accepted 23 September 2000

Abstract

Disc brakes are exposed to large thermal stresses during routine braking and extraordinary thermal stresses during hard braking. High-*g* decelerations typical of passenger vehicles are known to generate temperatures as high as 900°C in a fraction of a second. These large temperature excursions have two possible outcomes: thermal shock that generates surface cracks; and/or large amounts of plastic deformation in the brake rotor. In the absence of thermal shock, a relatively small number of high-*g* braking cycles are found to generate macroscopic cracks running through the rotor thickness and along the radius of the disc brake. The analysis herein shows that rotor failure is a consequence of low cycle thermo-mechanical fatigue. An analysis of the vehicle dynamics was used to find a heat flux equation related to braking forces. The heat flux equation was then used in a finite element analysis to determine the temperature profile in the brake. Once the brake temperature was obtained, a simplified shrink fit analysis was used to estimate the stresses that arise during hard braking. This approach shows that plastic deformation occurs due to the large thermal strains associated with high-*g* braking. The calculated strain amplitude was then used in a Coffin–Manson law to predict the number of high-*g* braking cycles to failure. Good agreement was obtained between reported braking cycles to failure and the proposed theoretical approach

Keywords: Thermal fatigue; Heat cracks; Brake failures; Thermal stress; Fatigue

* Corresponding author. Tel.: +1-217-244-1016; fax: +1-217-333-1942.
E-mail address: t-machi@vivc.edu (T.J. Mackin).

[1]This paper was equal part of a group project assigned by Professor T.J. Mackin to a senior level class on Failure Analysis.

1350-6307/02/$ - see front matter
PII: S1350-6307(00)00037-6

1. Introduction

Thermal cracking is commonly observed in disc brake rotors following high-*g* braking events [1,2]. The cracks fall into two broad categories: a series of heat cracks that partially penetrate the surface of the discs [2]; and thru-cracks that completely pass through the disc wall. Though it is well known that thermal cracks do arise from hard braking [1], there is no formal treatment of the problem of thru-cracks. This paper presents a failure analysis of thermal cracking in disc brake rotors. The analysis was motivated by thermal cracking in the front disc brakes in a heavy duty Ford F-250 pickup truck (Fig. 1). The front brakes failed while the truck was hauling a trailer filled with cattle. Failure occurred after several stops, and was indicated by an audible 'ping' and a pronounced ticking sound during subsequent braking.

Disc brakes are fabricated from grey cast iron with the typical geometry shown in Fig. 2. Grey cast iron is chosen for its relatively high thermal conductivity, high thermal diffusivity and low cost. The brake rotor consists of a hat, or hub, which is connected to the wheel and axle, and an inboard and outboard braking surface. The outboard braking surface is attached directly to the hat, while the inboard braking surface is attached to the outboard unit by a series of cooling vanes. A small groove is machined around the periphery of the hat-rotor attachment site to relieve the stress concentration associated with the change in section. It is important to note that the inboard disc is not directly attached to the hat; *its only attachment to the hat is through the cooling vanes*. The inboard and outboard rotors are squeezed by the brake pads during braking. The subsequent frictional work arrests the rotation of the wheel and generates a substantial amount of heat. Braking events last on the order of seconds, generating frictional heating in the rotors while leaving the hat very near room temperature. Thermal cracking is not common in passenger vehicles but it *is* relatively common in trucks and emergency vehicles; the very sorts of vehicles that are exposed to extreme conditions. It is important to note that those conditions are not considered abusive, rather they simply expose the limitations of braking technology. Though the present article was motivated by failure of disc brakes on a truck, the following sections present a general treatment of the problem that is applicable to any vehicle.

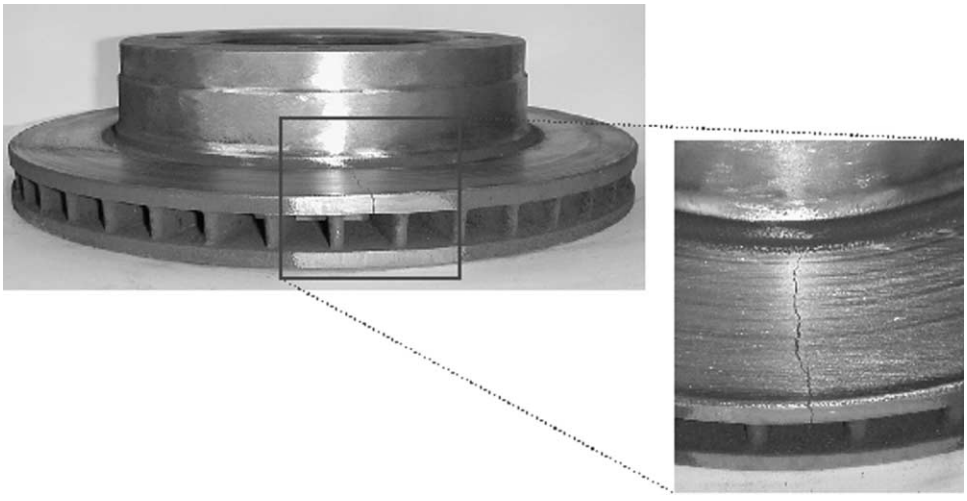

Fig. 1. Picture of a failed front brake rotor from a Ford F-250 Pickup truck. Cracks are seen to run radially from the hat to the exterior of the disc.

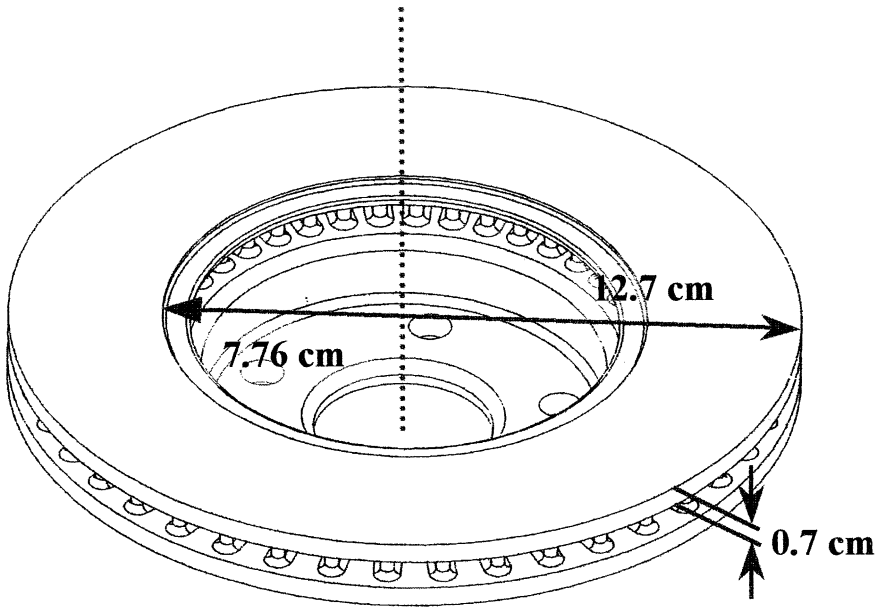

Fig. 2. Schematic of a typical passenger car brake rotor with dimensions used in the present analysis.

2. Vehicle dynamics

Braking must, necessarily, remove the kinetic energy of a moving vehicle in a timely and repeatable fashion. In order to estimate the temperatures that arise during braking, it is necessary to calculate the forces acting on the brake rotors. A typical vehicle schematic is shown in Fig. 3, from which a moment balance about the center of gravity provides the following:

$$F_{z1} = mg\frac{(b-\Delta x_2)\cos(\alpha) - h_G\sin(\alpha) - K_1V^2 - \frac{h_G}{g}\dot{V}}{l+\Delta x_1+\Delta x_2} \tag{1a}$$

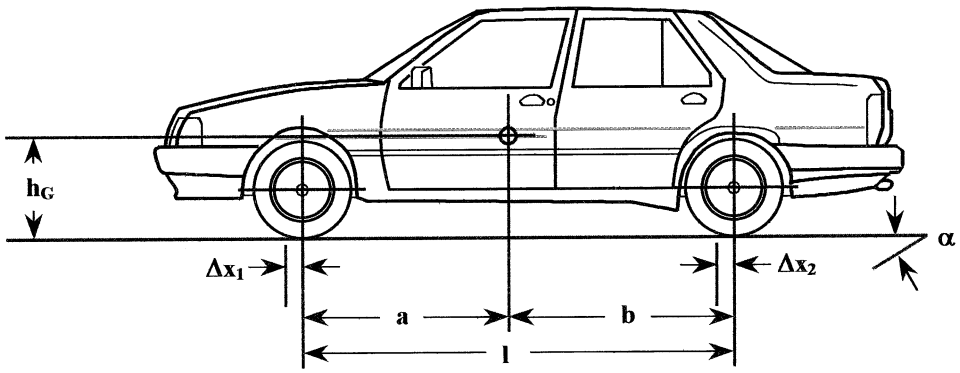

Fig. 3. Typical vehicle schematic with relevant dimensions.

$$F_{z2} = mg\frac{(a+\Delta x_2)\cos(\alpha) - h_G\sin(\alpha) - K_2V^2 - \frac{h_G}{g}\dot{V}}{l+\Delta x_1+\Delta x_2} \tag{1b}$$

where:

$$K_1 = \frac{\rho\times S}{2mg}\left[C_x h_G - lC_{M_y} + (b-\Delta x_2)C_z\right] \tag{2a}$$

$$K_2 = \frac{\rho\times S}{2mg}\left[C_x h_G - lC_{M_y} + (a+\Delta x_1)C_z\right] \tag{2b}$$

K_1 and K_2 are drag coefficients available in Genta [3], and all other symbols are as identified in Fig. 3.

Eqs. (1) can be further simplified by assuming that braking occurs on a perfectly flat surface ($\alpha=0$). Furthermore, the Δx terms measure the distances by which the tire normal forces shift from center. Since these Δx values are small compared with all other vehicle dimensions, these terms are dropped from Eqs. (1) and (2). The drag coefficients were found to amount to less than 1% of the load on each tire and were also ignored. As a result, Eqs. (1) reduce to the following simplified form:

$$F_{z1} = \frac{mg}{l}\left(b\frac{h_G}{g}\dot{V}\right) \tag{3a}$$

$$F_{z2} = \frac{mg}{l}\left(b\frac{h_G}{g}\dot{V}\right) \tag{3b}$$

Eqs. (3) show that the load distribution on the tires depends upon the distance of each tire from the center of gravity, and the acceleration of the vehicle. During deceleration, the load shifts to the front tires so that a large fraction of the work-of-braking is done by the front brakes. Most cars are outfitted with a proportioning valve that meters the hydraulic force applied to the front and rear brakes, reducing the deceleration of the vehicle and generating a 60/40 front/rear load distribution on the tires. A 60/40 load-ratio was used for the subsequent braking analysis. A free-body diagram of a front tire–rotor system, (Fig. 4), is used to derive the following equations of equilibrium:

$$\sum F_y = N - W = ma_y = 0 \tag{4a}$$

$$\sum F_x = F_{axel} - 2F_{rotor} + F_{tire} = ma_x \tag{4b}$$

$$\sum M_0 = r_{rotor}(2F_{rotor}) + r_{tire}(F_{tire}) = I_{rotor}\alpha \tag{4c}$$

Since 60% of the braking load is borne by the front brakes, that amount of kinetic energy into a single disc is given by [4,5]:

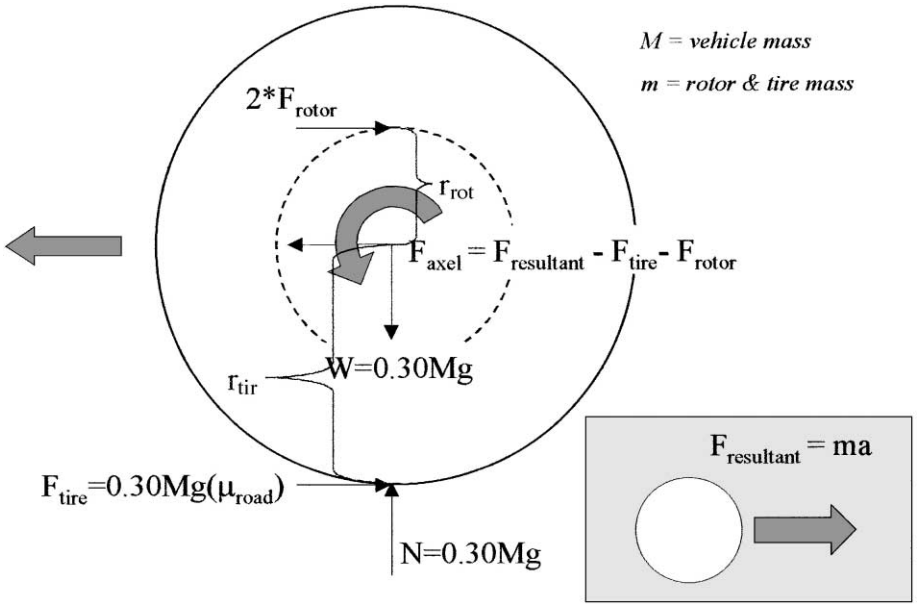

Fig. 4. Free body diagram of an automotive wheel.

$$0.3\cdot\frac{1}{2}M_0^2 =_{\text{dissipated}}= \int P_{\text{dissipated}}(t)\mathrm{d}t = \int (2F_{\text{rotor}})v_{\text{rotor}}(t)\mathrm{d}t \tag{5}$$

The power dissipated by each rotor face is equal to the instantaneous heat flux into the rotor face. Such a relationship can be used to predict the magnitude of the temperature excursions seen in the rotors. The energy balance equation can be used to this end, utilizing the following kinematic relationships for constant acceleration:

$$\left.\begin{aligned} V_{\text{vehicle}} = (t) &= v_{\text{initial,vehicle}} - at \quad a = \frac{v_{\text{initial,vehicle}}}{t_{\text{stop}}} \\ \frac{V_{\text{vehicle}}(t)}{r_{\text{tire}}} &= \omega(t) = \frac{v_{\text{rotor}}}{r_{\text{rotor}}} \end{aligned}\right\} v_{\text{rotor}}(t) = \frac{r_{\text{rotor}}}{r_{\text{tire}}}\left(v_{\text{initial,vehicle}} - \left\{\frac{v_{\text{initial,vehicle}}}{t_{\text{stop}}}\right\}\right) \tag{6}$$

F_{rotor} is constant with respect to time, and $v_{\text{rotor}}(t)$ varies only linearly with time so the energy balance equation becomes:

$$0.3\cdot\frac{1}{2}Mv_0^2 = (2F_{\text{rotor}})\int_0^{t_{\text{stop}}} v_{\text{rotor}}(t)\mathrm{d}t = (2F_{\text{rotor}})\frac{r_{\text{rotor}}}{r_{\text{tire}}}\left(v_0 t_{\text{stop}} - \frac{1}{2}\left\{\frac{v_0}{t_{\text{stop}}}\right\}t_{\text{stop}}^2\right) \tag{7}$$

Industry representatives have stated that a typical hard braking event is one that takes a vehicle from 45 m/s to a dead stop in 6 s. Experiments on a simulation rig have shown that 300 cycles of such braking are sufficient to generate thermal cracks in a brake rotor. The rotor force for a typical vehicle is calculated using the vehicle data contained in Table 1, resulting in:

Table 1
Vehicle data

Vehicle mass, M	1500 kg
Initial velocity, V_0	45 m/s
Time to stop, t_{stop}	6 s
Effective rotor radius, r_{rotor}	0.10 m
Tire radius, r_{tire}	0.38 m

$$F_{rotor}\frac{(30\%)\cdot\frac{1}{2}\cdot Mv_0^2}{2\cdot\frac{r_{rotor}}{r_{tire}}\cdot\left(v_0\cdot t_{stop}-\frac{1}{2}\left\{\frac{v_0}{t_{stop}}\right\}t_{stop}^2\right)} \tag{8}$$

The instantaneous heat flux into the rotor face is directly calculated using the following:

$$\dot{Q}_{in}(t)=(F_{rotor})v_{rotor}(t)=(6412N)\frac{r_{rotor}}{r_{tire}}\left(v_0-\left\{\frac{v_0}{t_{stop}}\right\}t\right) \tag{9}$$

$$\dot{Q}_{in}(t)=75{,}938W-\left(12{,}656\frac{W}{s}\right)t$$

Finally, the total rotor force applied to both the inboard and outboard rotors can be used to calculate the caliper clamping force required to stop the vehicle. The magnitude of the clamping force is found using Coulombic friction, where μ is about 0.4:

$$F_{caliper}=\frac{F_{rotor}}{\mu_{pad}}\approx 16{,}000N \tag{10}$$

This force generates a clamping stress in the brake rotor while the rotor force generates a shear stress. Brake pads typically cover a 60° swath along the rotor. In the present case this results in a contact area of $A=53$ cm^2. Using this area and the forces calculated Eqs. (8) and (10), the rotor stresses that arise from the mechanics of braking are given by:

$$\sigma_3=2\text{ MPa}$$

$$\tau=1.2\text{ MPa} \tag{11}$$

2.1. Material properties

The automotive industry typically utilizes flake cast irons in braking applications [6–8]. Hardness tests were conducted on the rotor depicted in Fig. 1 to determine the exact iron alloy. Three measurements each were made on the hat region, the outboard rotor and the inboard rotor. Several trends emerged: first, the hardest material is found on the inboard rotor (97 HRB), followed by the outboard rotor (94 HRB), and, finally, the hat (88 HRB). A statistical comparison of these data shows that each region has hardness that

is significantly different from each other region. These hardness differences are expected to arise from the differential cooling rates associated with the casting process and are not thought to arise from the thermal transients associated with braking. The measured Rockwell-B hardness values correspond to Brinell hardness in the range of 170–220 HB, placing the UTS on the order of 400 MPa [6]. A comparison with handbook data on cast irons identifies the present alloy as a GG25 cast iron [6]. The key material properties for this alloy are listed in Table 2.

A sample section was cut from the brake rotor for micro-structural evaluation (Fig. 5). The sample was cut from the outside toward the inside using an oil-cooled band saw. Significant residual tensile stresses were noted during sample machining: *the first cut resulted in a partial fracture through a 1cm wide section of the brake when the saw was within that distance of the inner radius*. The fracture was accompanied by an audible 'ping' and the saw cut was seen to open by several millimeters (Fig. 5). The wider cut in Fig. 5 shows the initial slice through the rotor. The second cut reveals the actual width made by the saw, while the opening of the initial cut includes displacement associated with the relief of residual tensile hoop stresses. The sample section was polished and etched using a 5% nital solution, and the microstructure was examined at several points on the brake sample, denoted as locations 1, 2, and 3 in Fig. 5. The microstructures confirm that the brake material is a flake graphite (Fig. 6). In addition to graphite flakes, the low magnification images of Fig. 6 also show spherical inclusions consistent with slag contamination during casting. These inclusions are not intended to be present and will have a detrimental effect on the thermal performance of the brake. The measured differences in hardness with location on the brake correspond with the microstructures shown in Fig. 6, where the higher hardness regions exhibit fine pearlite.

3. Estimated braking temperatures

A finite element analysis was conducted to obtain an estimate of the temperature distribution in the brake rotor. Radial symmetry was assumed, and a one-degree section of the rotor was chosen as a representative volume and meshed into roughly 50 elements. A stepped heat flux was applied to the brake surface in contact with the pad. The surface adjacent to the hub and the cross-sectional surfaces were insulated due to radial symmetry. Convection was applied to the other surfaces in a stepped manner, with the film convection coefficient decreasing from 30 W/m^2 K at each successive time step to simulate the decrease in angular velocity of the rotor over the braking cycle. The initial temperature of the rotor was set to 300 K. A transient analysis was performed over an interval of 6 s, in half-second time steps using the heat flux formula given by Eq. (9b). The resulting curve was integrated over each 1/2 second interval and each of those values was divided by the area of the brake pad for input into a heat flux table (J/m^2). A plot of the temperature profile through the width of the outboard rotor after 2.5 s of braking is shown in Fig. 7.

4. Estimating the lifetime of the brake disc

Braking causes rapid heating of rotor surface that can lead to thermal shock in the skin of the brake [2]. That problem can be treated using the method of stress suppression [9] to calculate the stresses in the skin

Table 2
Parameters for estimating fatigue lifetime

Material	Brinnel hardness	σ_y (MPa)	E (GPa)	σ_f'	b	ε_f'	c
GG25 #4	174	215	90	241	−0.115	0.008	−0.360

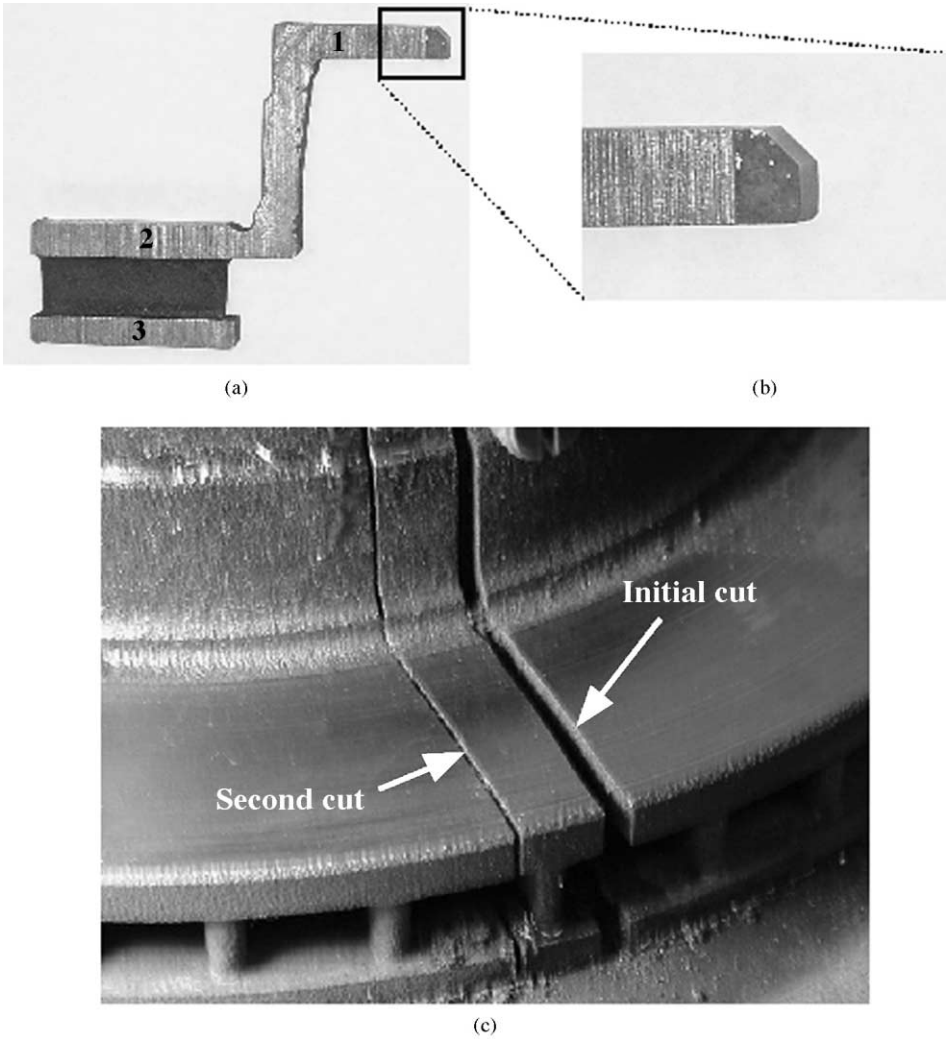

Fig. 5. Views of the Ford F-250 disc brake: (a) cross-section of the brake; (b) close-up of a fracture that occurred while machining the sample section; (c) comparison of the first and second cuts used to remove the cross-section shows considerable stress relief during machining.

of the disc. In addition to that problem, braking leads to rapid heating of the rotor with little or no change in the temperature of the hat. As such, the hat constrains the outboard braking surface. The following treatment ignores thermal shock in the rotor skin and concentrates on the thermal stress generated between the rotors and the hat. We approximate the stresses in the disc brake assembly by assuming that the hat remains at room temperature and constrains the thermal displacement of the outboard rotor. Furthermore, the hat was modeled as a solid rather than an open-walled cylinder. The constraint offered by the hat is akin to an internal pressure on the annulus of the outboard rotor and generates considerable constraint stresses in the outboard rotor. As a first approximation we ignore the effect of the inboard rotor and its vane attachments to the outboard side. Though this represents a considerable simplification, the results obtained are in good agreement with experience and experiment.

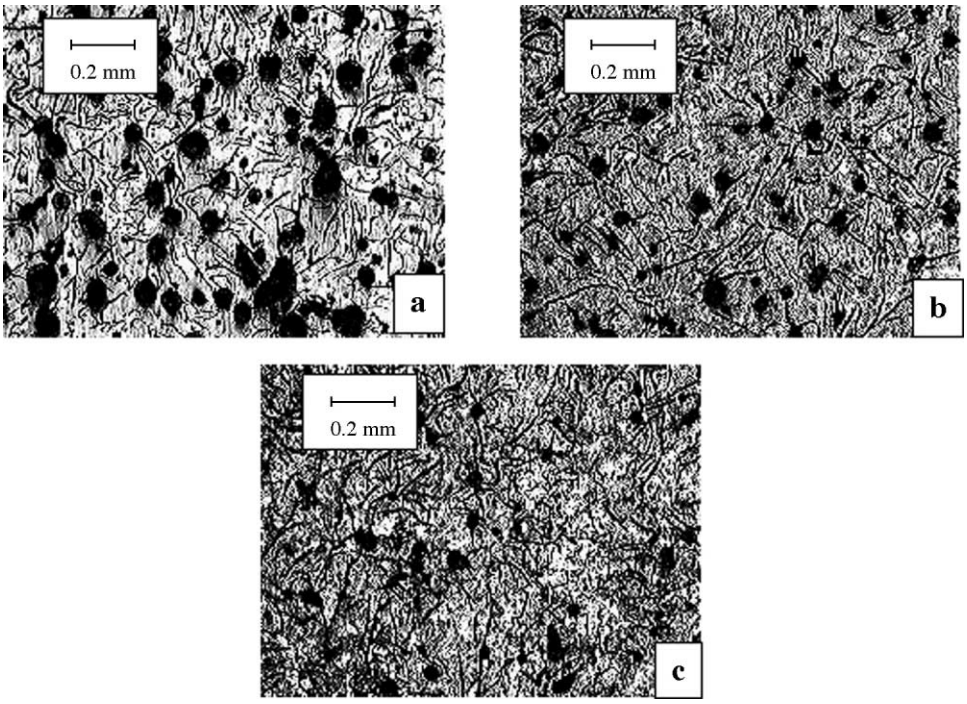

Fig. 6. Micrographs at several locations along the sample cross-section show the flake graphite structure along with carbide nodules: (a) center of hub; (b) center of outboard brake surface; (c) center of inboard brake surface.

The constraint of the hub prevents the free expansion of the rotor and is modeled as a two-element shrink fit (Fig. 8). In the absence of constraint, the outboard rotor would freely expand by an amount:

$$\Delta b = b\alpha\Delta T \tag{12}$$

However, this thermal expansion is constrained by the hat so that the total deflection is shared between an elastic outward displacement of the hat and an inward deflection of the rotor. Following [10], the inward deflection of an internally pressurized body (in this case the rotor) is given by:

$$\Delta b = \left(\frac{P}{E}\right) b\left\{\left(\frac{a^2+b^2}{a^2-b^2}\right)+\nu\right\} \tag{13}$$

where the symbols are defined in Fig. 8. Likewise, the outward deflection of the hat, would be given by:

$$\Delta c = \frac{P}{E}\cdot c\cdot(1-\nu) \tag{14}$$

The sum of these deflections must be equal to the free thermal deflection of the rotor, as follows:

$$\alpha\Delta T b = \Delta c + \Delta b \tag{15}$$

At the interface of the hat and rotor, $c = b$, so that:

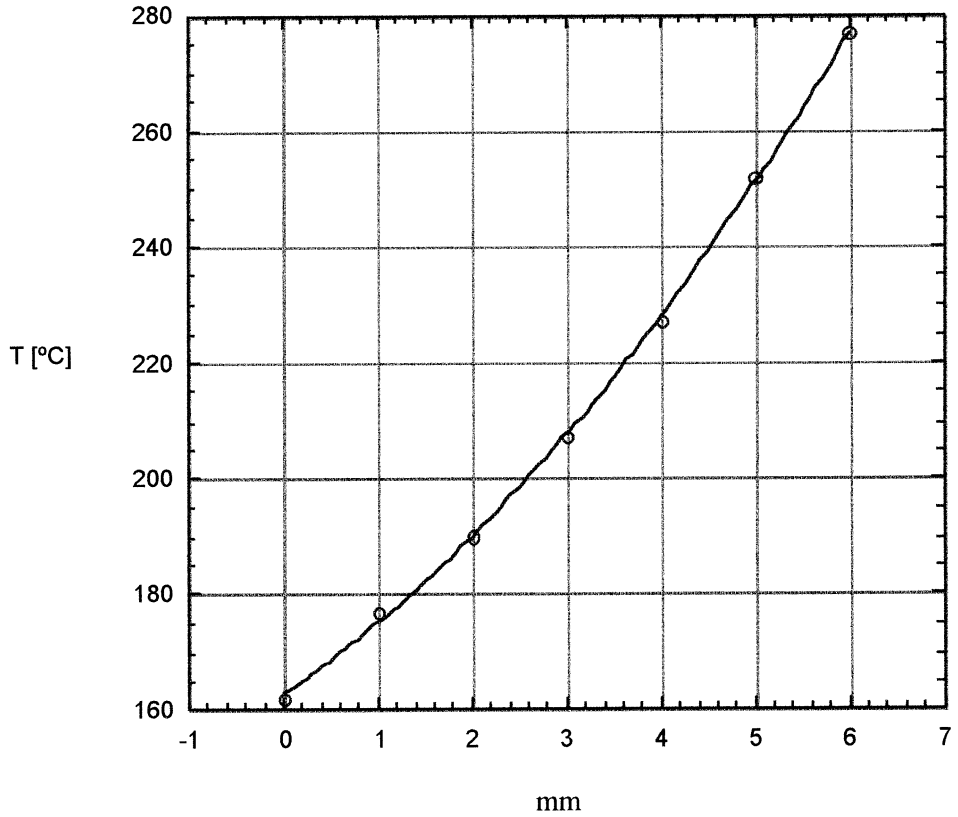

Fig. 7. Computed temperature profile through the thickness of the outboard rotor.

$$\alpha \Delta T \cdot b = \frac{P}{E} \cdot b \cdot (1 - \nu) + \frac{P}{E} b \left[\left(\frac{a^2 + b^2}{a^2 - b^2} \right) + \nu \right] \tag{16}$$

which is re-arranged to provide the constraint pressure:

$$P = \alpha \Delta T E \left[\left(\frac{a^2 + b^2}{a^2 - b^2} \right) + 1 \right]^{-1} \tag{17}$$

To arrive at an approximation for the constraint pressure generated by the hat, we utilize the average temperature through the thickness of the rotor at time $t = 2.5$ s (Fig. 7). The average increase in rotor temperature is roughly 220°C, generating a constraint pressure of approximately 100 MPa. This constraint pressure generates stresses in the hoop and radial directions according to:

$$\sigma_1 = \frac{-Pb^2(a^2 + r^2)}{r^2(a^2 - b^2)} \tag{18}$$

$$\sigma_2 = \frac{Pb^2(a^2 - r^2)}{r^2(a^2 - b^2)} \tag{19}$$

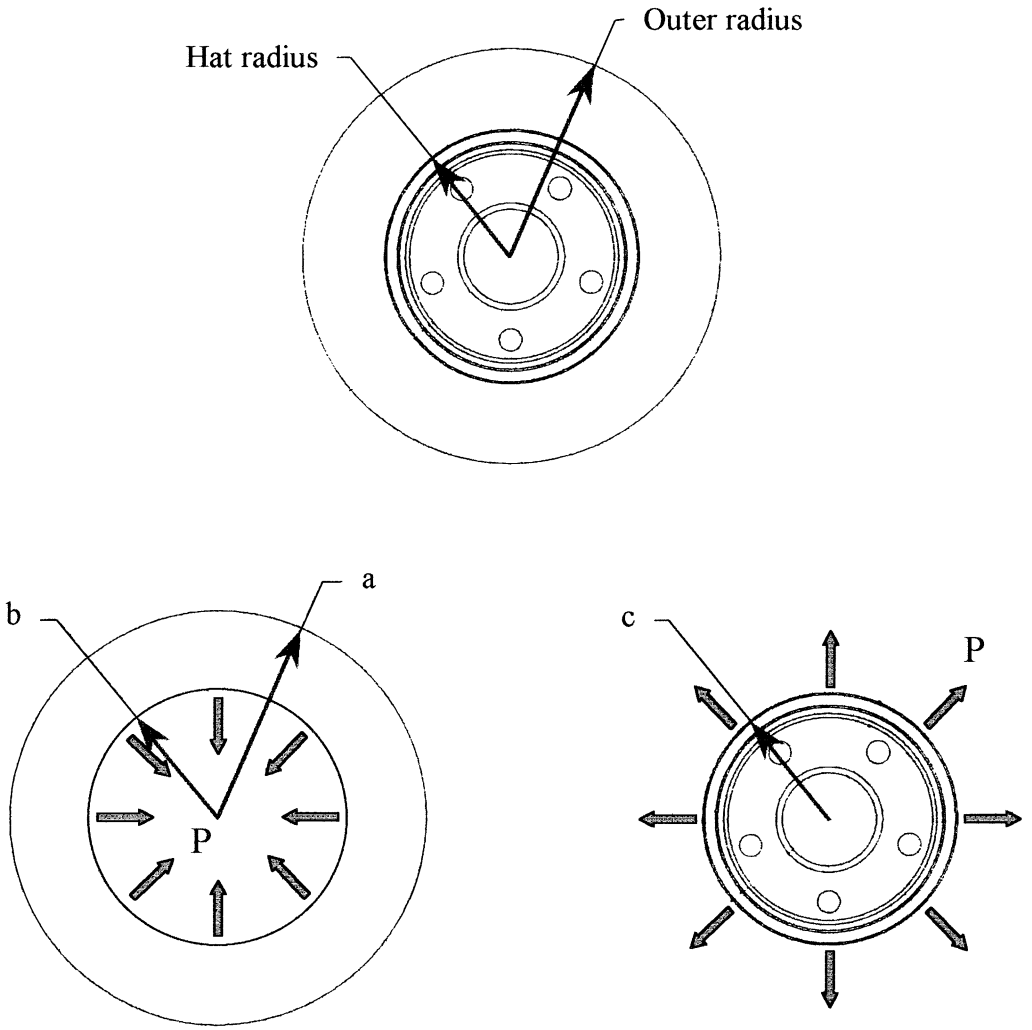

Fig. 8. Schematic of the brake rotor illustrating the overall view of the brake (upper), the internal pressure on the disc (bottom left), and the external restraining pressure from the hat (bottom right) generated by thermal stresses.

where σ_1 is the hoop stress, and σ_2 is the radial stress.

Plots of these stresses as well as the equivalent von Mises stress are shown in Fig. 9. Fig. 9 reveals that the mean equivalent stress is roughly 180 MPa. Recall that the GG25 cast iron alloy has a yield strength of 215 MPa and elastic modulus of 90 GPa. A close look at Fig. 9 shows that the braking temperatures generate thermal stresses that clearly exceed the yield strength adjacent to the hub and extending about 1 cm outward from the hub. Furthermore, the rotor yields in compression upon braking, while a residual tensile hoop stress sets in upon cooling. This cycling between compression and tension, in phase with the temperature of the brakes, is the thermo-mechanical mechanism responsible for failure. Accounting for the constraint afforded by the cooling fins makes the matter worse because the fins would further restrict the thermal deformation of the rotor. The braking stresses shown in Eqs. (11) would also increase the equivalent stress and

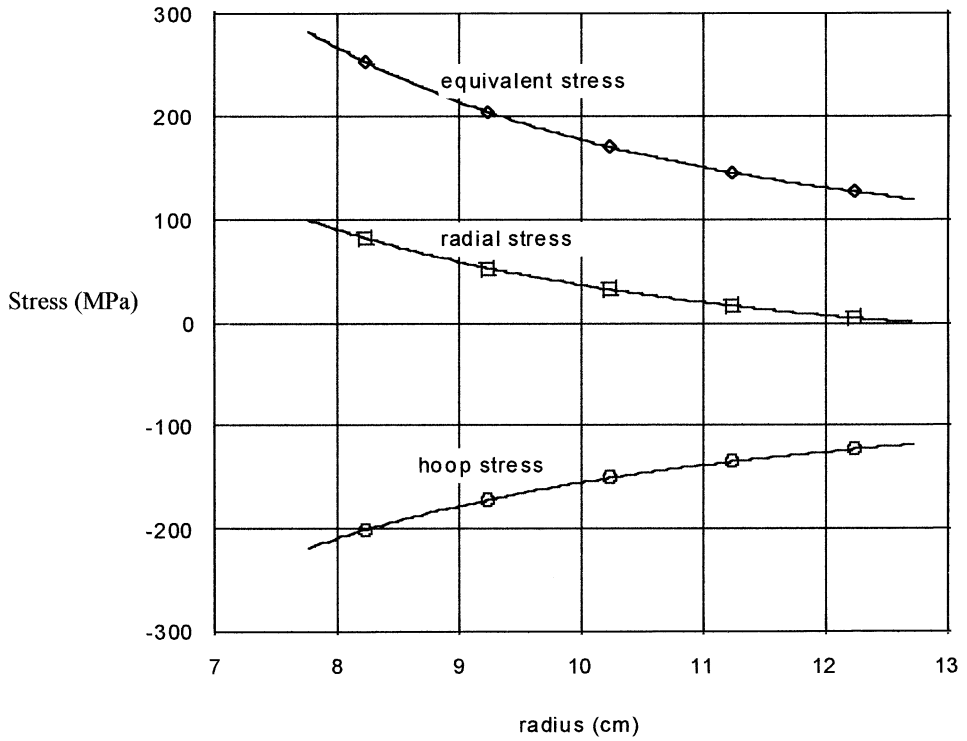

Fig. 9. Plot of the radial, hoop, and equivalent stresses in the brake rotor resulting from the shrink-fit model.

further drive plastic deformation during braking. One could use the method of stress suppression to include the thru-thickness thermal gradient as well. This, again, would increase the equivalent stress and hasten the demise of the disc.

In order to estimate of the fatigue lifetime of the rotor, we utilize the Coffin–Manson law, where:

$$\varepsilon_a = \sigma_f' N_f^b + \varepsilon_f' N_f^c \tag{20}$$

The empirical constants are identified as:

ε_a is the applied strain amplitude,
σ_f' is the stress amplitude coefficient,
ε_f' is the strain amplitude coefficient,
N_f is the number of cycles to failure.

The applied strain amplitude is estimated by calculating the elastic strain associated with the average equivalent rotor stress of 180 MPa, giving $\varepsilon_a = 0.2\%$. The fatigue lifetime is found by plotting Eq. (20) over a broad range of strain amplitudes, (Fig. 10), using the fatigue constants for a GG25 cast iron alloy, shown in Table 2. As shown in Fig. 10, the fatigue lifetime associated with $\varepsilon_a = 0.2\%$ is approximately 333 cycles to failure. Remarkably, experiments at Ford Motor Company have found that failure under the specified braking conditions occurs at roughly 300 braking cycles.

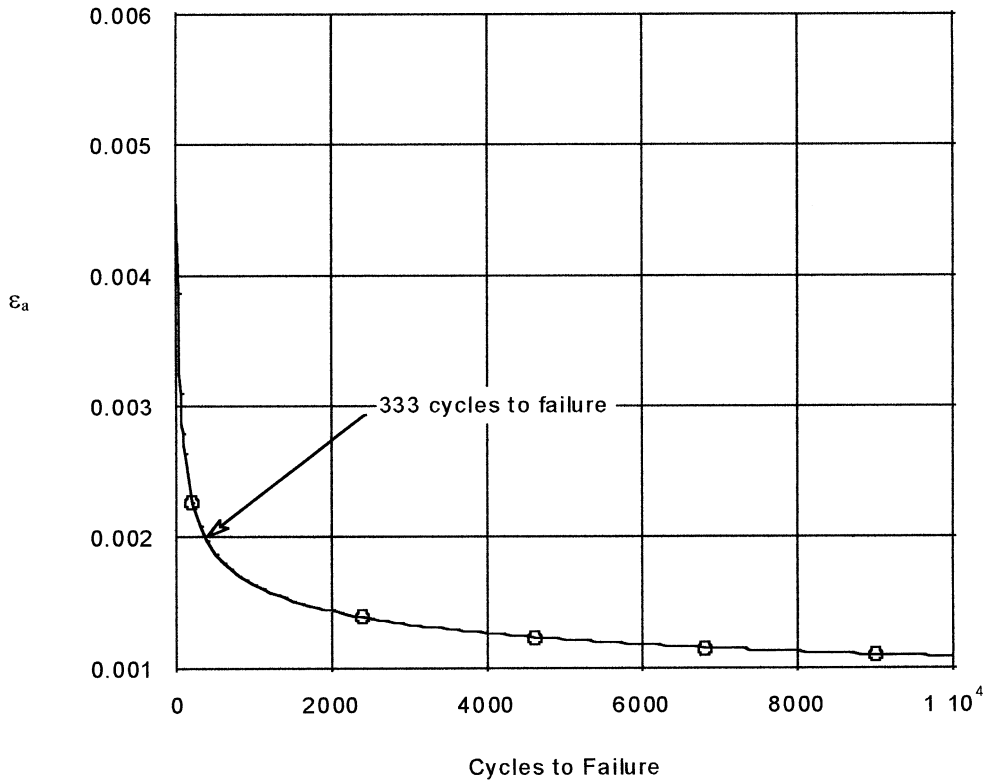

Fig. 10. Plot of the Coffin–Manson law for a GG25 cast iron alloy. An applied strain amplitude of 0.2% provides an estimated life of 333 cycles.

5. Conclusions

Thermal cracking in disc brake rotors is a low cycle thermo-mechanical fatigue problem. The frictional work of braking rapidly heats the rotors while having no effect on the hat region. This difference in temperatures sets up compressive thermal stresses in the rotor during braking that reverse sign upon cooling. Thermo-mechanical stresses were calculated using a simple shrink-fit analysis wherein the hat was modeled as constraining the free thermal expansion of the rotor. These stresses were found to exceed the yield strength in the rotor over considerable distances from the hub and were very near the yield strength over most of the rotor. Following cool down a tensile residual stress, at or very near the yield strength, is set into the rotor. Subsequent braking cycles the rotor through an applied stress range that has an amplitude near that of the yield strength of the rotor, leading to a design problem of low cycle fatigue. Such high stress/strain amplitudes are modeled using the Coffin–Manson law. In the present study, the strain amplitude is simply calculated using the elastic strain associated with an average thermo-mechanical stress amplitude. This approach shows that thermal cracking can be expected in a relatively small number of high-*g* braking cycles.

There are three ways to eliminate thermal cracking in brake rotors: (1) increase the yield and fatigue strength of the rotor material; (2) decrease the braking temperatures; and/or (3) re-design the hub–rotor unit to eliminate constraint stresses. New brake materials have been identified that can operate at substantially higher temperatures [2]. However, this leads to a need for heat shielding around the brakes, the use of higher temperature bearing materials and a radical re-design of the entire brake assembly. Advanced

designs that incorporate cooling into the brakes are also difficult to achieve and add considerable cost to the brake unit [11]. The simplest approach is to eliminate the constraint brought about by the rotor–hub assembly [11]. The challenge of a new mechanical design that relieves the thermal constraint is left as an open invitation to the reader.

References

[1] Gunther, B, Klingelhoeffer, H. A systematic study for fatigue life prediction of grey cast iron disc brakes. In: Fatigue 2000. p. 397–405.
[2] Jimbo, Y, Mibe, T, Akiyama, K, Matsui, H, Yoshida, M, Ozawa, A. Development of high thermal conductivity cast iron for brake disc rotors. SAE Technical Paper #900002, 1990.
[3] Genta G. Motor vehicle dynamics: modeling and simulation. River Edge (NJ): World Scientific, 1997.
[4] Newcombe TP. Temperatures reached in disc brakes. J Mechanical Engineering Science 1960;2(3).
[5] Noyes, RN, Vickers, PT. Prediction of surface temperatures in passenger car disc brakes. SAE Technical Paper # 690457, 1969.
[6] Walton, CF, Editor. Iron castings handbook. Iron Castings Society, Inc., 1981.
[7] Nayar A. The metals data book. New York: McGraw-Hill, 1997.
[8] Anon. Metals handbook, vols. 1 and 10. 10th ed. ASM International, 1990.
[9] Timoshenko S. Strength of materials, part II. Krieger Publishing, 1983.
[10] Timoshenko SP, Goodier, JN. Theory of elasticity. McGraw-Hill, 1970.
[11] Metzler H. The brake rotor — friction partner of brake linings. SAE Technical Paper # 900847, 1990.